

A Comparative Study of Helical-Type and Traditional-Type Artery Bypass Grafts: Numerical Simulation

JUN WEN,* TINGHUI ZHENG,* WENTAO JIANG,* XIAOYAN DENG,† AND YUBO FAN†

Preliminary studies on an individual helical graft indicated that its hemodynamics might be improved while pressure drop increased compared with a traditional graft. Aiming to investigate whether the benefits of a helical graft to hemodynamics dominate its deficits, this study numerically carried out comparative study of helical-type artery bypass graft (ABG) and traditional-type ABG under both steady and pulsatile flow conditions. The results showed that a helical-type ABG resulted in reduced oscillating shear index, improved wall shear stress, enhanced flow mixing and three-dimensionality, and improved flow behavior at the distal anastomosis and occluded section of the host vessel compared with traditional-type ABG. More important, although a helical-type ABG did increase the pressure drop compared with a traditional one, its maximum percentage increase during a cardiac cycle was <21% which is still within physiological sense. Therefore, we believe that the adoption of helical bypass could help to prevent intimal hyperplasia (IH) and thrombosis at the distal anastomosis and improve the graft patency while keeping clinical maintenance. This investigation provided an important basis for the clinical applications and theory support of helical graft. *ASAIO Journal* 2011; 57:399–406.

It is well accepted that hemodynamics analysis is very important in the design of small caliber grafts.¹ The hemodynamics including local flow characteristics and wall shear stress (WSS) distribution is strongly influenced by the geometry configuration of the blood vessel.² Being man-made, it is possible to directly influence the grafts hemodynamics through improved design.³ Furthermore, both synthetic and autologous grafts need to take their configuration into consideration. Accordingly, in recent years, optimal graft design has been an objective of much research and is a natural end-point for the study of correlations between hemodynamics and graft failure.³

Inspired by the nonplanar geometries, which are widely existed in human circulation system, exploration to the nonplanar geometries such as S-type grafts was proposed.^{4,5} Com-

pared with traditional planar grafts, these nonplanar graft configurations resulted in improved hemodynamic environments including promoted flow mixing and reduced stagnation flow (low shear) regions. However, these grafts also increased host artery vessels injury and often constrained by surgical considerations beyond hemodynamics.^{6,3}

In an attempt to induce nonplanar flow effects that could be maintained in clinical settings, Caro *et al.*⁷ proposed the use of helical grafts to create swirling flow referring to aortic arch. Although preliminary studies^{8–11} suggested that helical conduit appeared promising in preventing intimal hyperplasia (IH) and thrombosis but increased the pressure drop, namely, the blood resistance, compared with a traditional graft, which may lead to nonenough downstream perfusion.¹² So far, the role played by flow helicity in vascular hemodynamics is still much debated, Whether the benefits of a helical graft to hemodynamics dominate its deficits needs to be further investigated, and the operation difficulties raised by its geometry complication need to be solved before its real clinical application.

The research on traditional artery bypass graft (ABG) indicated that the flows in graft and artery interact with each other, and different suture techniques at anastomoses or graft-artery connections have important impact on the graft flow field. In addition, IH at the distal anastomosis, which is especially prominent at the heel, toe, along the suture line, and on host artery bed, is the major factor responsible for bypass graft failure.¹³ However, up to now, all the research on helical grafts focused on the graft itself, no detailed analysis of the anastomotic flow was reported, and no research was carried out to study the flow characteristics of a complete helical-type ABG. Therefore, to gain a better view of the effect of swirling flow in a small caliber graft, this study numerically carried out a comparative study of a helical-type ABG and a traditional one under both steady and pulsatile flow conditions. Traditional hemodynamic parameters such as WSS, oscillating shear index (OSI), and velocity vectors were calculated for the comparison. Pressure drops along ABG, which is important to graft patency, were investigated in detail. In addition, the helicity of flow by means of Lagrangian approach was introduced as a quantitative index of flow three-dimensionality and flow mixing.

Model and Methods

Model Geometry

The geometry was built using software Pro/E 5.0. The traditional graft followed the arc of a circle between the anastomosis, whereas the helical graft adopted the circle arc as its guide cylinder axis, as shown in **Figure 1**. Accordingly,

From the *Department of Applied Mechanics, Sichuan University, Chengdu; and †School of Biological Science and Medical Engineering, Beihang University, Beijing, China.

Submitted for consideration October 2010; accepted for publication in revised form May 2011.

Tinghui Zheng and Jun Wen both contributed equally to the article. Reprint Requests: Yubo Fan, PhD, Key Laboratory for Biomechanics and Mechanobiology of Ministry of Education, School of Biological Science and Medical Engineering, Beihang University, XueYuan Road No.37, HaiDian District, Beijing 100191, China. Email: yubofan@buaa.edu.cn.

DOI: 10.1097/MAT.0b013e3182246e0a

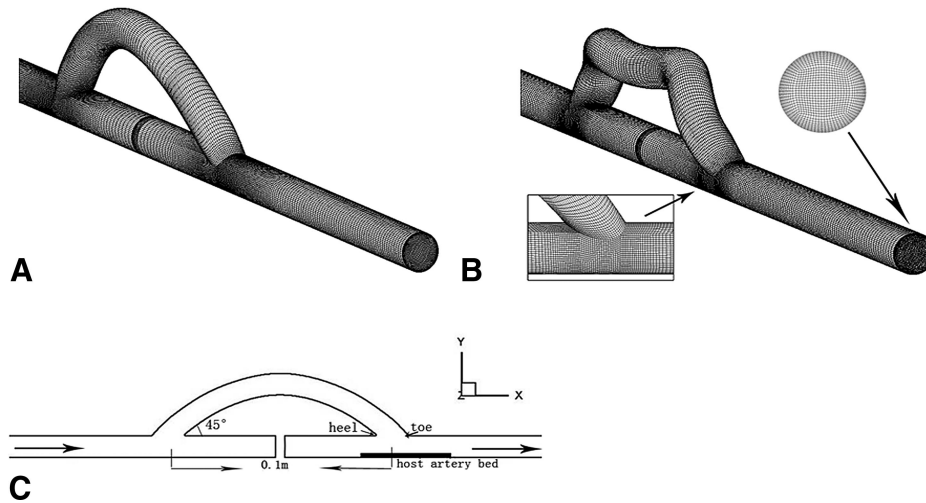


Figure 1. Artery bypass graft (ABG) configurations with numerical grid marked on vessel surfaces. Particulars of the meshes for cross-section and distal anastomosis were presented. A viscous layer of 0.1 D was imposed adjacent to the vessel wall to capture the boundary layer, and meshes were refined at the anastomosis: **(A)** traditional-type ABG; **(B)** helical-type ABG; and **(C)** symmetry plane of the traditional-type ABG. The definitions referred to in the text are indicated. The arrows represent the flow direction.

no more artery injury or operation difficulty was increased in helical-type ABG. To make a fair comparison, both grafts made angles of 45° with the fully occluded host arteries at both end-to-side junctions. All the internal diameters of grafts and arteries were set at 6 mm; the pitch and amplitude of the one-turn helical graft were 30 mm and 1.5 mm, respectively. The host arteries were prolonged 20 D upstream and downstream, respectively, to ensure fully developed entrance and exit flow.

The mesh generation was done in software ICEM. In constructing the computational domain, viscous layers of 0.1 D were imposed adjacent to the vessel walls to capture the boundary layer, and meshes were refined at the anastomosis.

Helical Flow Quantification

Recently, helicity was effectively used to quantify the helical structure of blood flow.^{13–18} The density per unit volume of kinetic helicity is defined as¹⁹:

$$H_k(s;t) = \vec{V}(s;t) \cdot (\nabla \times \vec{V}(s;t)) = \vec{V}(s;t) \cdot \vec{\omega}(s;t) \quad (1)$$

Where \vec{V} is the velocity vector, $\vec{\omega}$ is the vorticity vector, s is the position of a particle, and t is the time.

Local normalized helicity (LNH), a nondimensional quantity which physically represents the angle between velocity and vorticity vectors, was introduced as a useful indicator of rotation direction:

$$\text{LNH}(s;t) = \frac{\vec{V}(s;t) \cdot \vec{\omega}(s;t)}{|\vec{V}(s;t)| |\vec{\omega}(s;t)|} \quad -1 \leq \text{LNH} \leq 1 \quad (2)$$

A zero LNH indicates a purely axial or circumferential flow, whereas the modulus of LNH becomes 1 in a purely helical flow.^{15,16} If the trace described by the generic particle labeled k moving in a vessel is considered, its dynamics can be characterized by means of the following quantity¹⁴:

$$\text{hfi}_k = \frac{1}{N_k} \sum_{j=1}^{N_k} |\text{LNH}|_j \quad 0 \leq \text{hfi}_k \leq 1 \quad (3)$$

Where N_k is the number of points j , ($j = 1, \dots, N_k$) in the k th trajectory.

The helical flow index (HFI), a synthetic value which is linear inverse to OSI, was calculated over a set of particles moving into the fluid¹⁵

$$\text{HFI} = \frac{1}{N_p} \sum_{k=1}^{N_p} \text{hfi}_k = \frac{1}{N_p} \sum_{k=1}^{N_p} \frac{1}{N_k} \sum_{j=1}^{N_k} |\text{LNH}|_j \quad 0 \leq \text{HFI} \leq 1 \quad (4)$$

Where N_k is the number of points j , ($j = 1, \dots, N_k$) in the k th trajectory, and N_p is the number of particles in which the quantity LNH was calculated.

Oscillating Shear Index

The OSI, which denotes the changed frequency of the WSS direction, is defined as

$$\text{OSI} = 0.5 \left[1 - \frac{\left| \int_0^T \text{WSS}(s, t) dt \right|}{\int_0^T |\text{WSS}(s, t)| dt} \right] \quad 0 \leq \text{OSI} \leq 0.5 \quad (5)$$

Where s is the position on the vessel wall, and T is the cardiac cycle time of the pulsatile flow. A zero OSI corresponds to unidirectional shear flow, whereas a high OSI value denotes the direction of the WSS vector changes frequently, which has been related to IH.²⁰

Governing Equations

Because the shear rate in most part of the flow field in this study was over 100 s^{-1} , blood was assumed to be isotropic, homogeneous, incompressible and Newtonian with a constant dynamic viscosity of $3.5 \times 10^{-3} \text{ kg/m} \cdot \text{s}$ and a density of 1050 kg/m^3 , respectively. The corresponding governing equations are given as follows:

$$\rho \partial \vec{u} / \partial t + \rho (\vec{u} \cdot \nabla) \vec{u} + \nabla p - \mu \Delta \vec{u} = 0 \quad (6)$$

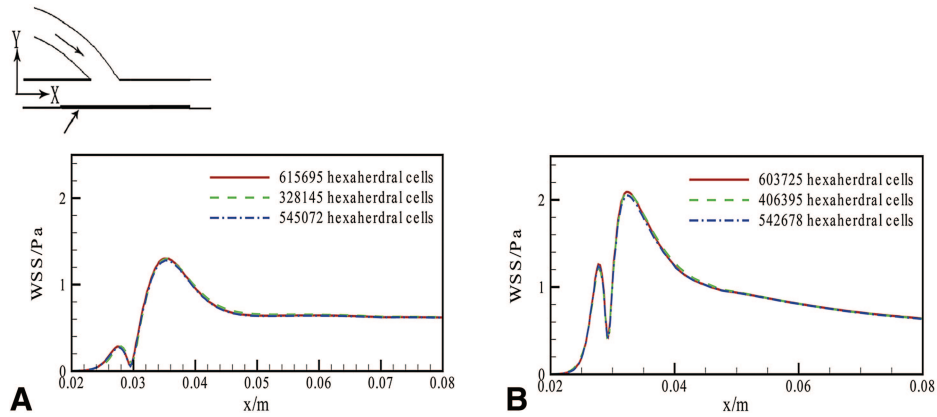


Figure 2. Grid refinement study: The wall shear stress (WSS) distributions along the host artery beds were presented at two different meshes: **(A)** traditional-type artery bypass graft (ABG); **(B)** helical-type ABG.

$$\nabla \cdot u = 0 \tag{7}$$

Where \vec{u} and p represent the fluid velocity vector and the pressure, respectively. ρ and μ are the density and dynamic viscosity of blood, respectively.

Boundary Conditions

The inlet velocity was set 0.144 m/s for the steady flow simulation, and the corresponding Reynolds number based on graft diameter and blood viscosity was 260. A native coronary waveform was specified as the inflow boundary for pulsatile flow simulation,²¹ its maximum Reynolds number during the cycle is 612. Assuming a heart rate of 80 beats/min, the period of each cycle is 0.75 seconds.

The export boundary condition was defined as outflow. The graft and vessel wall were assumed to be rigid and nonslip.

Numerical Simulation

Grid refinement studies were carried out for both configurations under steady flow condition. The WSS distributions along the artery floor were presented at three different meshes in **Figure 2**. The maximum relative errors between the medium and fine meshes are <3%. Therefore, the medium grid were considered satisfactory and adopted for the following investigation.

The study on time step for unsteady flow was carried out, and finally, each pulse cycle was divided into 300 time steps of size 2.5 ms. In addition, four cardiac cycles were performed for each simulation to eradicate any start-up effects and achieve stable results.

The flow visualization and analysis were completed by the commercial CFD software Fluent 6.0, which was based on the finite volume method, default Segregate Implicit 3D Solver was adopted. Discretization of the equations involved a second order upwind differencing scheme. SIMPLEC was adopted for the pressure velocity correction, and the residual error convergence threshold was set as 1e-5.

Results

Steady-State Flow

The WSS contour maps in the complete ABG models (**Figure 3A and B**) show that the WSS magnitude in a helical-

type ABG was not only increased in its graft segment but also at its anastomosis region, especially near its suture line and on its artery bed. The WSS distributions along the axial lines of artery beds (**Figure 2**) hold similar general characters for two ABG models and gradually became to consistent with each other when distally away from the distal anastomosis. However, quantitatively, the WSS values of the helical-type ABG were remarkably larger than those in the traditional-type ABG.

The WSS contour maps on host artery beds where the horizontal axis of the map represents the axial distance along the host vessel, whereas the vertical axis represents the circumferential distance along the host vessel wall, which were presented in **Figure 3, C and D**. In addition, it was indicated that the WSS was symmetrically distributed in the traditional-type ABG, whereas asymmetrically in the helical-type ABG. The low-WSS region (smaller than 0.6 Pa) in the helical-type ABG was proximally displaced, which indicated elevated shear stress levels in the occluded host vessel region, when compared with the traditional-type model.

Figure 4 shows the axial components of velocity vectors superimposed the contour maps of velocity magnitude in the symmetry planes, and the recirculation regions were zoomed in. It was observed that the helical-type ABG improved the axial velocity at its distal anastomosis while reduced the size of stagnation and recirculation flow zone, when compared with the traditional-type ABG.

Three cross-sections at the distal anastomosis were chosen to show the cross-flow streamlines and flow velocity contours: C_1 represents the mean section; C_3 represents the toe section; and C_2 represents the mean section of C_1 and C_3 . Symmetrical flow was kept in the traditional-type ABG. Also, two Dean Vortices were visible at its C_3 section, and stagnation zones near the suture line appeared on its C_1 and C_2 sections. The out-of-plane geometry of helical graft broke the flow symmetry, and a stronger clockwise vortex accompanying with a weaker counter-clockwise vortex were observed at all selected sections, which helped to avoid flow stagnation. When flowing downstream, the vortex cores in helical-type ABG moved to the centerline of its host artery, and the strength of two vortices gradually became equal (**Figure 5**).

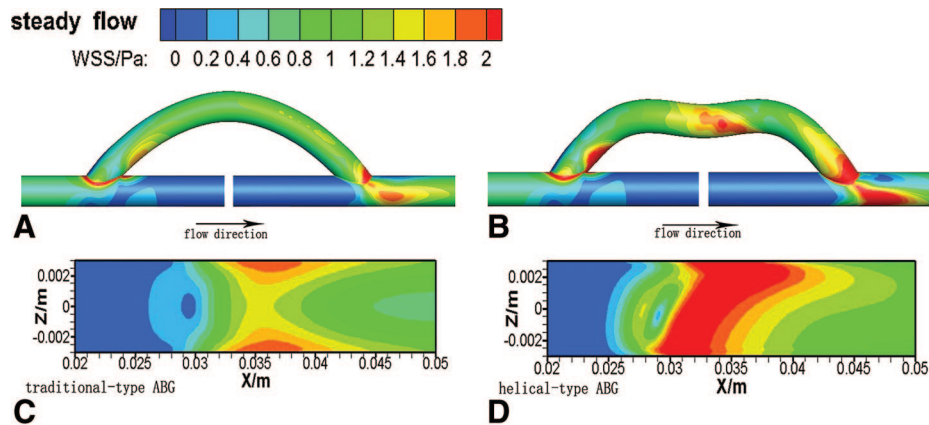


Figure 3. **A** and **B:** The contour maps of wall shear stress (WSS) in artery bypass grafts (ABGs). The arrows represent the flow direction. WSS magnitude was not only improved in helical graft segment but also at its distal anastomosis, when compared with the traditional-type ABG. **C** and **D:** The WSS contour maps on host artery beds where the horizontal axis represents the axial distance along the host vessel, whereas the vertical axis represents the circumferential distance along the host vessel wall. WSS was symmetrically distributed in the traditional-type ABG, whereas asymmetrically in the helical-type ABG. The low-WSS region (smaller than 0.6 Pa) in the helical-type ABG was proximally displaced, which indicates elevated shear stress levels in its occluded host vessel region, when compared with the traditional model.

Pulsatile Flow

The local values of OSI at the distal anastomosis were presented in **Figure 6**. When compared with the traditional model, the helical graft significantly reduced the region size of high OSI, decreased the maximum OSI at the distal anastomosis by 58.4%, in contrast to a decrease of 5.2% in the occluded region.

To have a better view of the effect of helical bypass on pressure drop, 11 slices of the configurations as shown in **Figure 7** were chosen for the calculation of the area-averaged pressures at four moments: a) systolic acceleration; b) maximum velocity; c) minimum velocity; and d) diastole. The pressure drop varied with time and reached maximum at systole, whereas minimum at diastole. Generally, the helical bypass did increase the pressure drop compared with the traditional-type ABG, and the percentage increase varied with cycle. The maximum percentage increase of 20.6% happened at moment of maximum velocity, and the pressure drop along helical bypass was 1.5 mm Hg. Noteworthy, the pressure drops along two ABGs at systole were consistent with each other.

Figure 8 presented the views of the evolution of particle sets emitted at different time moments. Color coding of the particle traces was used to display the instantaneous positive (negative) value of the LNH. Although because of the geometry alteration, 3D flow was induced at the proximal anastomosis in the traditional-type ABG, few flow mixing happened, and the helicity of near-wall flow was quite low. However, as the flow moved through the helical graft, the momentum of the fluid caused it to follow the graft wall curvature, thus near-wall flow was kept highly 3D, and flow mixing was significantly improved. The rotation of flow continued after reentering the downstream host artery.

Figure 9 presented the HFI values calculated over traces of particle sets emitted at the four time instants T_j over the time interval $T_{es} - T_j$, and the percent distribution of particle traces with respect to the hfi_k , i.e., the average LNH of each trajectory of particles. Helical-type ABG exhibited hfi_k percent distributions with low degree of asymmetry, whereas traditional-type ABG presented high asymmetry, especially at time T_3 and T_4 . All the trajectories had flat distribution except that the one in traditional-type ABG emitted at T_4 . The HFIs of helical-type

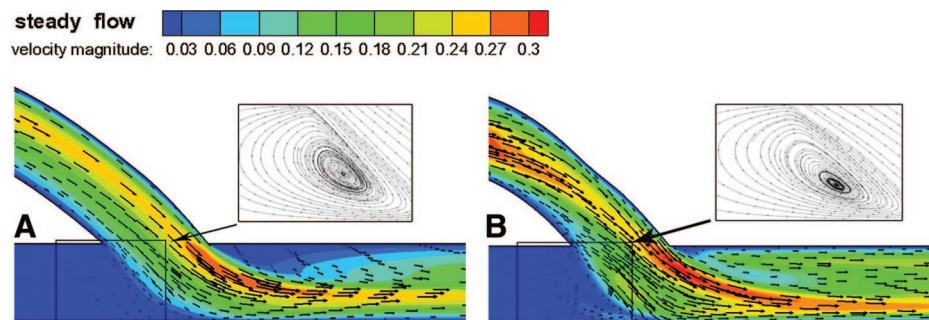


Figure 4. The contour maps of velocity magnitude superimposed with the axial velocity vectors, particulars of recirculation flow zone were presented. **A:** Traditional-type artery bypass graft (ABG); **(B)** helical-type ABG. The axial velocity at the distal anastomosis was increased, and the size of stagnation and recirculation flow zone was reduced in the helical-type ABG compared with traditional-type ABG.

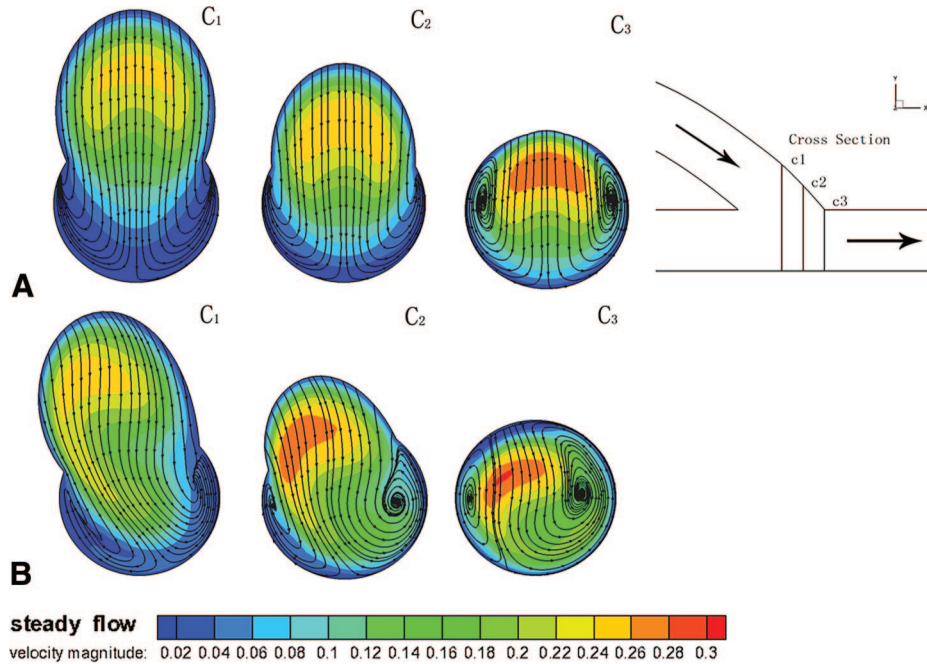


Figure 5. Three cross-sections at the distal anastomosis were chosen to show the cross-flow streamlines. C_1 represents the mean section; C_3 represents the toe section; C_2 represents the mean section of C_1 and C_3 : **(A)** the traditional-type artery bypass graft (ABG); **(B)** the helical-type ABG. Symmetrical flow was kept in the traditional model, and two Dean Vortices were visible at its C_3 section, whereas stagnation zone near the suture line appeared on its C_1 and C_2 sections. The out-of-plane geometry of helical graft broke the flow symmetry, and a stronger clockwise vortex accompanying with a weaker counter-clockwise vortex were observed at all selected sections, which helped to avoid flow stagnation. As flowing downstream, the vortex cores in helical-type ABG moved to the centerline of its host artery, and the strength of two vortices gradually became equal.

ABG were increased, when compared with the traditional-type ABG at all moments, and the percentage increase reached 28% at time T_4 . In addition, the maximum hfi_k in the helical-type ABG was 0.831, in contrast to 0.643 in the traditional-type ABG.

Discussion

The aim of this investigation is to find out whether a helical-type ABG is hemodynamically beneficial to ABG patency, when compared with the traditional-type ABG, and the investigation focused on the distal anastomosis region, which is

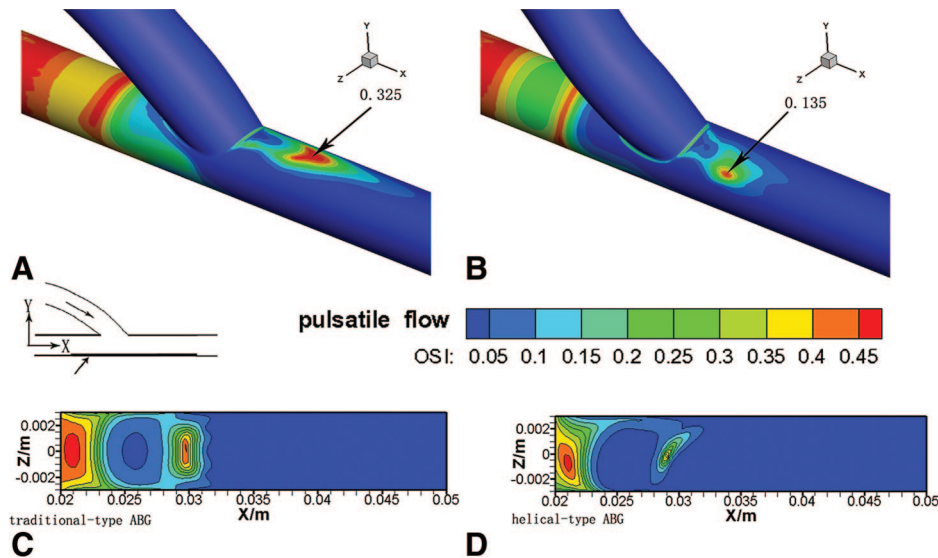


Figure 6. A and B: The oscillating shear index (OSI) contour maps at the distal anastosis; **(C, D)** the OSI contour maps on the host artery beds which coordinates are the same with Figure 3. As it shown that helical bypass reduced the size of high OSI region, when compared with the traditional-type artery bypass graft (ABG). In addition, the maximum OSI value in helical-type ABG decreased 58.4% at the distal anastomosis, in contrast to a decrease of 5.2% in the occluded region.

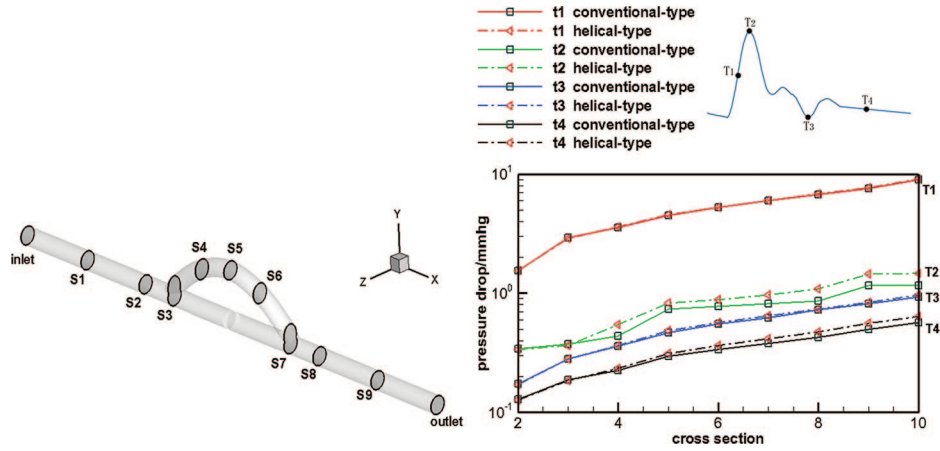


Figure 7. The area-averaged pressures of 11 cross-sections shown above were adopted to compute the pressure drop along the artery bypass graft (ABG) at four time moments. T1: Systolic acceleration; T2: maximum velocity; T3: minimum velocity; and T4: diastole. The pressure drop varied with time and reached maximum at systole, whereas minimum at diastole. Generally, the helical bypass did increase the pressure drop compared with the traditional-type ABG, and the percentage increase varied with cycle. The maximum percentage increase of 20.6% happened at moment of maximum velocity, and the pressure drop along helical bypass was 1.5 mm Hg. Noteworthy, the pressure drops along two ABGs at systole were consistent with each other.

most prone to IH. Although no quantitative relationship between the hemodynamic parameters and IH is found, there is, however, a trend relationship between the local flow field and IH. It has been demonstrated that IH tends to occur preferentially in regions of low time averaged shear stress and long particle residence time.²² It has also been suggested a connection between the spatial gradient and sharp temporal variation of WSS and regions where IH preferentially develops.²³

The geometric features of an ABG directly affected its hemodynamic performance: 1) the loop shape of the traditional graft is semicircular in contrast to the “M-shaped” loop of helical graft. Consequently, the WSS and OSI profiles along the helical loop were approximately diametrically opposed, with the high and low zones rotating with axial position; 2) The insertion of the helical graft was rotated slightly counter clockwise relative to the traditional

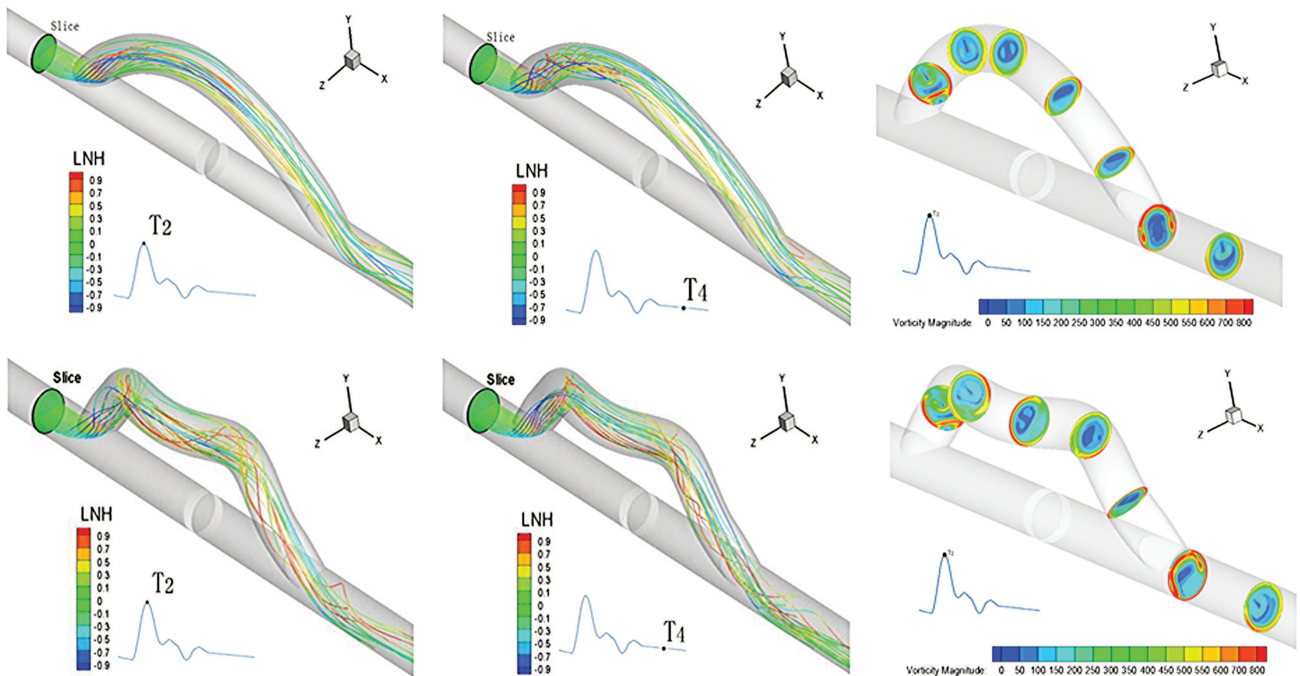


Figure 8. Views of the evolution of particle sets emitted at different time moments. Color coding of the particle traces was used to display the instantaneous positive (negative) value of the local normalized helicity (LNH). Although because of the geometry alteration 3D flow was induced at the proximal anastomosis in the traditional-type artery bypass graft (ABG), few flow mixing happened, and the helicity of near-wall flow was quite low. However, as the flow moved through the helical graft, the momentum of the fluid caused it to follow the graft wall curvature, thus near-wall flow was kept highly 3D, and flow mixing was significantly improved. The rotation of flow continued after reentering the downstream host artery.

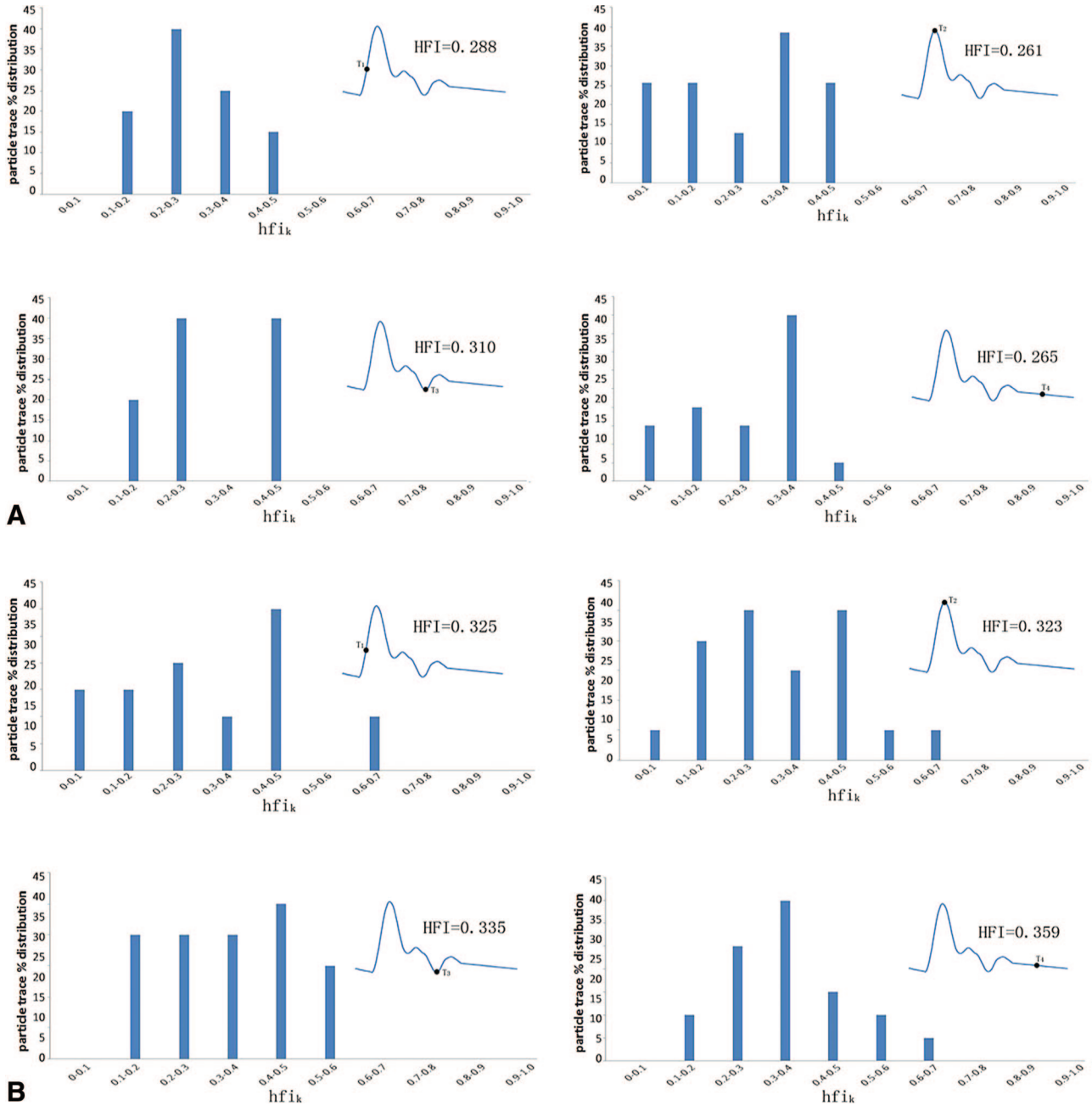


Figure 9. The helical flow index (HFI) values calculated over traces of particle sets emitted at the four time instants, T_j , over the time interval $T_{es} - T_j$ and the percent distribution of particle traces with respect to the hfi_k , i.e., the average LNH of each trajectory of particles: **(A)** traditional-type artery bypass graft (ABG); **(B)** helical-type ABG. Helical-type ABG exhibited hfi_k percent distributions with low degree of asymmetry, whereas traditional bypass presented high asymmetry especially at time T_3 and T_4 . All the trajectories had flat distribution except that the one in the traditional-type ABG emitted at T_4 . The HFIs of the helical-type ABG were increased compared with the traditional one at all moments, and the percentage increase reached 28% at time T_4 . In addition, the maximum hfi_k in the helical-type ABG was 0.831, in contrast to 0.643 in the traditional-type ABG.

graft when looking from downstream end (**Figure 1**). Consequently, symmetric flow was kept at the distal anastomosis of the traditional-type ABG, whereas asymmetric flow patterns and WSS distribution emerged at the anastomosis of the helical-type ABG. On the whole, the geometry of the helical-type ABG is out of plane in contrast to the in-plane geometry of the traditional-type ABG. Consequently, three-dimensional flow and flow swirling were significantly

strengthened in the helical-type ABG. The increased flow helicity especially of the near-wall flow and strong secondary flow facilitated the mixing of particle between the near-wall region and core of the flow in the helical-type ABG, which brought the high-momentum fluid to the surface and retarded the onset of flow separation. Furthermore, the forward streaming blood curled by the swirling flow in the helical-type ABG filled the space left by the flow separation

at the inner wall, which helped to eliminate stagnation flow regions and mechanical trauma to blood cells.

In this study, the level of shear stress involved was on the order of 2 dynes/cm², which was much lower than 50 dynes/cm², the threshold to activate platelets and induce platelet aggregation. In this case, the elevated WSS may lead to a reduction in the concentration of platelets near the vessel wall possibly through a mechanism of the Magnus effect^{24,25} that induces forces on platelets and pushes them away from the vessel wall. In addition, the swirling flow-induced in-plane mixing would further lower the concentration of platelets near the wall and suppressed the interaction of platelets with the wall of ABG.

As indicated by the study on individual helical grafts, the magnitude of the pressure drop along a helical graft was considerably increased compared with a traditional one, which might prevent its medical application. However, according to the present investigation, although the helical-type ABG increased the pressure drop compared with the traditional one, its maximum percentage increase was <21%, which is still within physiological sense and can be overcome by optimal geometry design.

In addition, compared with cylindrical tube, the structural property of a helical tube improved resistance to kinking when subjected to bending moments, which helps to guarantee its graft geometry *in vivo*,⁹ and the graft artery junction of a helical-type ABG is similar to the traditional type, which will not increase operation difficulty and artery injury.

In a summary, desirable high WSS, low OSI, and increased flow swirling were achieved in the helical-type ABG. We, therefore, may expect that a helical-type ABG may decrease the likelihood of platelets adhesion, clot formation, and thrombosis in the graft surface and reduce the possibility of IH at the distal anastomosis.

The graft and vessel wall in the present investigation were assumed to be rigid and nonslip, which is not true *in vivo*. However, previous studies indicate that the wall elasticity may be of considerable significance in transport mechanisms but of somewhat lesser importance as far as the gross features of the flow is concerned.²⁶ This study helped to increase our understanding of the flow mechanism in helical-type ABG and provided an important basis for its clinical applications and theory support.

Acknowledgment

Supported by the National Natural Science Foundation of China (10925208 and 11072162) and "863" High Technology Project.

References

1. Chiu JJ, Chen LJ, Lee CL, Chien S: Mechanisms of induction of endothelial cell E-selectin expression by smooth muscle cells and its inhibition by shear stress. *Blood* 110: 519–528, 2007.
2. O'Flynn PM, O'Sullivan G, Pandit AS: Methods for three-dimensional geometric characterization of the arterial vasculature. *Ann Biomed Eng* 35: 1368–1381, 2007.
3. Loth F, Fischer PF, Bassiouny HS, et al: Blood flow in end-to-side anastomoses. *Annu Rev Fluid Mech* 40: 367–393, 2008.
4. Fan YB, Xu ZP, Jiang WT, et al: An S-type bypass can improve the hemodynamics in the bypassed arteries and suppress intimal hyperplasia along the host artery floor. *J Biomech* 41: 2498–2505, 2008.
5. Papaharilaou Y, Doorly DJ, Sherwin SJ: The influence of out-of-plane geometry on pulsatile flow within a distal end-to-side anastomosis. *J Biomech* 35: 1225–1239, 2002.
6. Giordana S, Sherwin SJ, Peiro J, et al: Local and global geometric influence on steady flow in distal anastomoses of peripheral bypass grafts. *J Biomech Eng* 127: 1087–1098, 2005.
7. Caro CG, Nick JC, Nick W: Preliminary comparative study of small amplitude helical and traditional ePTFE arteriovenous shunts in pigs. *J R Soc Interface* 2: 261–266, 2005.
8. Coppola G, Caro C: Oxygen mass transfer in a model three-dimensional artery. *J R Soc* 5: 1067–1075, 2008.
9. Cookson AN, Doorly DJ, Sherwin SJ: Mixing through stirring of steady flow in small amplitude helical tubes. *Ann Biomed Eng* 37: 710–721, 2009.
10. Chen Z, Fan YB, Deng XY, Xu Z: Swirling flow can suppress flow disturbances in endovascular stents: A numerical study. *ASAIO J* 55: 543–549, 2009.
11. Zhan F, Fan YB, Deng XY: Swirling flow created in a glass tube suppressed platelet adhesion to the surface of the tube: Its implication in the design of small-caliber arterial grafts. *Thromb Res* 125: 413–418, 2010.
12. Zheng TH, Fan YB, Xiong Y, et al: Hemodynamics performance study on small diameter helical grafts. *ASAIO J* 55: 192–199, 2009.
13. Cole JS, Watterson JK, Reilly O: Numerical investigation of the haemodynamics at a patched arterial bypass anastomosis. *Med Eng Phys* 24: 393–401, 2002.
14. Grigioni M, Daniele C, Morbiducci U, et al: A mathematical description of blood spiral flow in vessels: Application to a numerical study of flow in arterial bending. *J Biomech* 38: 1375–1386, 2005.
15. Morbiducci U, Ponzini R, Grigioni M, Redael A: Helical flow as fluid dynamic signature for atherogenesis risk in aortic coronary bypass. A numeric study. *J Biomech* 40: 519–534, 2007.
16. Morbiducci U, Ponzini R, Nobili M, et al: Blood damage safety of prosthetic heart valves. Shear induced platelet activation and local flow dynamics: A fluid-structure interaction approach. *J Biomech* 42: 1952–1960, 2009.
17. Morbiducci U, Ponzini R, Rizzo G, et al: In vivo quantification of helical blood flow in human aorta by time-resolved three-dimensional cine phase contrast MRI. *Ann Biomed Eng* 37: 516–531, 2009.
18. Shadden SC, Astorino A, Gerbeau JF: Computational analysis of an aortic valve jet with Lagrangian coherent structures. *Chaos* 20: 017512, 2010.
19. Belian A, Chkhetiani O, Golbraikh E, Moiseev S: Helical turbulence: Turbulent viscosity and instability of the second moments. *Physica A* 258: 55–68, 1998.
20. Ku DN: Blood flow in arteries. *Annu Rev Fluid Mech* 29: 399–434, 1997.
21. Politis AK, Stavropoulos GP, Christolis MN, et al: Numerical modeling of simulated blood flow in idealized composite arterial coronary grafts: Transient flow. *J Biomech* 41: 25–39, 2008.
22. Bassiouny H, White S, Glagov S, et al: Anastomotic intimal hyperplasia: Mechanical injury or flow induced. *J Vasc Surg* 15: 708–717, 1992.
23. Lei M, Kleinstreuer C, Archie J: Haemodynamic simulation and computer-aided designs of graft-artery junctions. *ASME J Biomech Eng* 119: 343–348, 1997.
24. Schoephoerster RT, Oynes F, Nunez G, et al: Effects of local geometry and fluid dynamics on regional platelet deposition on artificial surfaces. *Arterioscler Thromb* 13: 1806–1813, 1993.
25. Vaughn HR, Reis GE: A magnus theory. *AIAA J* 11: 1396–1403, 1973.
26. Jou LD, Berger SA: Numerical simulation of the flow in the carotid bifurcation. *Theor Comp Fluid Dyn* 10: 239–248, 1998.